distance d_1 for four different frequencies. Both the magnitude and phase of $\Gamma_{\rm in}$ reveal the oscillatory behaviors when $d_1 < 1.5\lambda$ at 15, 20, and 24 GHz. Our additional computation indicates that a small gap between the dielectric slab and flanged coaxial line introduces significant changes in $\Gamma_{\rm in}$.

III. Conclusion

The problem of a flanged-coaxial line radiation into a dielectric slab is investigated using the Hankel transform and mode-matching technique. The behaviors of reflection in terms of frequency, coaxial line geometry, slab permittivity, and thickness are shown. Our solution is rigorous, yet in rapidly convergent series, which are efficient for numerical computation.

References

[1] M. Stuchly and S. Stuchly, "Coaxial line reflection methods for measuring dielectric properties of biological substances at radio and microwave frequencies—A review," *IEEE Trans. Instrum. Meas.*, vol. IM-29, pp. 176–183, Sept. 1980.

[2] D. Misra, "A quasi-static analysis of the open-ended coaxial line," *IEEE Trans. Microwave Theory Tech.*, vol. MTT-35, pp. 925–928, Oct. 1987.

[3] J. Mosig, J. C. Besson, M. Gex-Fabry, and F. Gardiol, "Reflection of an open-ended coaxial line and application to nondestructive measurement of materials," *IEEE Trans. Instrum. Meas.*, vol. IM-30, pp. 46–51, Mar. 1981.

[4] S. Fan, K. Staebel, and S. Stuchly, "Static analysis of an open-ended coaxial line terminated by layered media," *IEEE Trans. Instrum. Meas.*, vol. IM-39, pp. 435–437, Apr. 1990.

[5] S. Bakhtiari, S. I. Ganchev, and R. Zoughi, "Analysis of radiation from an open-ended coaxial line into stratified dielectrics," *IEEE Trans. Microwave Theory Tech.*, vol. 42, pp. 1261–1267, July 1994.

[6] D. Misra, M. Chabbra, B. Epstein, M. Mirotznik, and K. Foster, "Noninvasive electrical characterization of materials at microwave frequency using an open-ended coaxial line: Test of an improved calibration technique," *IEEE Trans. Microwave Theory Tech.*, vol. 38, pp. 8–14, Jan. 1990.

[7] C. Pournaropoulos and D. K. Misra, "The co-axial aperture electromagnetic sensor and its application in material characterization," *Meas. Sci. Technol.*, pp. 1191–1202, 1997.

[8] D. K. Misra, "Evaluation of the complex permittivity of layered dielectric materials with the use of an open-ended coaxial line," *Microwave Opt. Technol. Lett.*, vol. 11, no. 4, pp. 183–187, Mar. 1996.

[9] ——, "On the measurement of the complex permittivity of materials by an open-ended coaxial probe," *IEEE Microwave Guided Wave Lett.*, vol. 5, pp. 161–163, May 1995.

[10] J. H. Lee, H. J. Eom, and K. H. Jun, "Reflection of a coaxial line radiating into a parallel plate," *IEEE Microwave Guided Wave Lett.*, vol. 6, pp. 135–137, Mar. 1996.

Vector Finite Hankel Transform Analysis of Shielded Single and Coupled Microstrip Ring Structures

Jen-Tsai Kuo

***Abstract*— The vector finite Hankel transform or the vector Bessel series expansion method is used to calculate the resonant frequencies of shielded single and coupled microstrip annular rings in a stratified dielectric structure. Vector global basis functions are employed to model the unknown currents on the ring conductors, and the calculations of their transforms are described. Calculated resonant frequencies for microstrip rings are presented and found to have good agreement with measurements.**

I. Introduction

Microstrip ring resonators have been widely used in various designs of microwave integrated circuits (MIC's) [1]. It is found that publications on rigorous analysis methods are limited. For open structures, a simple stationary formula is derived based on the reaction concept [2]. The vector Hankel transform (VHT) analysis method is found to be effective to deal with circular disks [3] and annular-ring [4] radiators. For closed structures with disk and ring resonators, an eigenfunction weighted boundary integral-equation method is developed in [5] to avoid the use of complicated spatial-domain Green's functions.

This work extends the full-wave VHT method [3], [4] to calculate the resonant frequencies of microstrip rings with metallic enclosure. The vector finite Hankel transform (VFHT) or the vector Bessel series (VBS) expansion method [6] is used to transform electromagnetic fields to the spectral (Hankel transform) domain. It is found that this technique has the following attractive features suitable for numerical calculations, similar but not limited, to those stated in [3]. First, it is not limited by the number and widths of metallic rings. Second, the spectral Green's functions can be easily obtained using the spectral immittance approach [7]. Third, algebraic equations, instead of coupled integral equations, are obtained for setting up the final determinantal equation. Fourth, vector global basis functions with proper edge conditions are employed to expand the unknown currents on the rings, and it results in a small-size matrix eigenvalue problem. Finally, the result for the resonant frequency is in a variational form.

This paper is organized as follows. Section II formulates the VFHT method for the analysis of microstrip rings embedded in a layered dielectric medium. The vector basis functions and their transforms used in this study are also described. In Section III, calculated results for single and coupled rings are presented and checked against published data and our measurements. Section IV presents conclusions.

II. Formulation

A. The VFHT and the Parseval's Relation

The cross section of the analyzed shielded coupled microstrip ring resonator is shown in Fig. 1. The rings are assumed to be

Manuscript received July 14, 1999. This work was supported in part by the National Science Council, R.O.C., under Contract NSC 88-2213-E-009-077.

The author is with the Department of Communication Engineering, National Chiao Tung University, 300 Taiwan, R.O.C. (e-mail: jtkuo@cc.nctu.edu.tw).

Publisher Item Identifier S 0018-9480(99)08796-7.

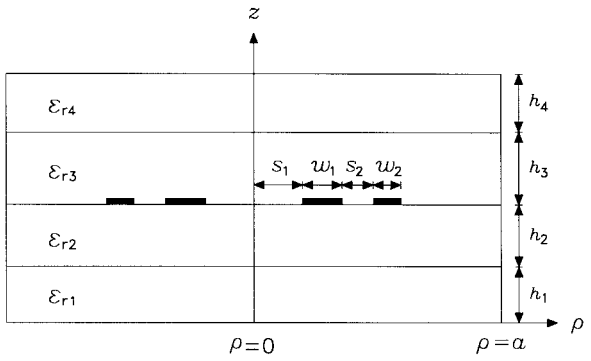

Fig. 1. Cross section of a coupled microstrip ring resonator.

perfectly conducting and infinitely thin. Starting with TE and TM to z formulation in the circular cylindrical coordinates and using the method of separation of variables, one can obtain the general solutions of the scalar potentials Φ^e (TM) and Φ^h (TE) in each layered dielectric region as

$$\Phi^{e,\,h} = e^{jn\phi}\sum_{m=1}^{\infty} S_m^{e,\,h}(z) J_n(\lambda_m^{e,\,h}\rho)/I_m^{e,\,h} \tag{1}$$

where n is the azimuthal resonance order, J_n is the nth-order Bessel function of the first kind, $\lambda_m^e = x_{nm}/a$ and $\lambda_n^h = x'_{nm}/a$ are the spectral variables for the TM and TE waves, respectively, and x_{nm} and x'_{nm} are the mth roots of $J_n(x)$ and $J'_n(x)$, respectively. $S_m^e(z)$ and $S_m^h(z)$ specify the z-dependence of the mth spectral waves, and $I_m^e = a|J'_n(x_m)|/\sqrt{2}$ and $I_m^h = a|J_n(x'_{nm})|\sqrt{(1-n^2/x'^2_{nm})/2}$. Each summation term in (1) is a cylindrical wave function with discrete eigenvalue for describing the electromagnetic fields inside a circular cylindrical waveguide [8]. With the $e^{jn\phi}$ factor being suppressed, the transversal E-fields can be written as

$$\begin{aligned}\begin{bmatrix} jE_\rho \\ E_\phi \end{bmatrix} &= \sum_{m=1}^{\infty}\begin{bmatrix} \dfrac{n}{\lambda_m^h\rho}\dfrac{J_n(\lambda_m^h\rho)}{I_m^h} & \dfrac{\partial}{\partial(\lambda_m^e\rho)}\dfrac{J_n(\lambda_m^e\rho)}{I_m^e} \\ \dfrac{\partial}{\partial(\lambda_m^h\rho)}\dfrac{J_n(\lambda_m^h\rho)}{I_m^h} & \dfrac{n}{\lambda_m^e\rho}\dfrac{J_n(\lambda_m^e\rho)}{I_m^e} \end{bmatrix} \\ &\quad\cdot\begin{bmatrix} S_m^h(z) \\ \dfrac{d}{dz}S_m^e(z)/\omega\varepsilon \end{bmatrix} \\ &\equiv \sum_{m=1}^{\infty}\overleftrightarrow{H}_m^{\mathrm{T}}(\rho)\begin{bmatrix} S_m^h(z) \\ \dfrac{d}{dz}S_m^e(z)/\omega\varepsilon \end{bmatrix}\end{aligned} \tag{2}$$

where $j = \sqrt{-1}$, and the superscript T stands for the transpose operation. The VFHT of $[jE_\rho E_\phi]^{\mathrm{T}}$ is defined as

$$\begin{bmatrix} \tilde{E}_m^h \\ \tilde{E}_m^e \end{bmatrix} \equiv \int_0^a \rho\ \overleftrightarrow{H}_m(\rho)\begin{bmatrix} jE_\rho \\ E_\phi \end{bmatrix} d\rho. \tag{3}$$

Substituting (2) into (3) and using the orthogonal relations between the cylindrical vector wave functions [8], one can verify that

$$\begin{bmatrix} \tilde{E}_m^h \\ \tilde{E}_m^e \end{bmatrix} = \begin{bmatrix} S_m^h(z) \\ \dfrac{d}{dz}S_m^e(z)/\omega\varepsilon \end{bmatrix}. \tag{4}$$

Similarly, the VFHT of the transversal H-fields $[jH_\phi\ {-}H_\rho]^{\mathrm{T}}$ is obtained as

$$\begin{bmatrix} \tilde{H}_m^h \\ \tilde{H}_m^e \end{bmatrix} = \begin{bmatrix} -\dfrac{d}{dz}S_m^h(z)/j\omega\mu \\ -jS_m^e(z) \end{bmatrix}. \tag{5}$$

The spectral-domain Green's functions, for the currents and transversal E-fields at $z = h_1 + h_2$, can be derived as follows. The functions $S_m^{e,\,h}(z)$ are expressed in terms of hyperbolic sin and cos functions weighted by m-dependent constants. The boundary conditions for transversal E- and H-fields should be applied to each dielectric interface and each ground plane. It can then be shown that $\tilde{E}_m^h = \tilde{Z}_m^h\tilde{J}_m^h$ and $\tilde{E}_m^e = \tilde{Z}_m^e\tilde{J}_m^e$, and $\tilde{Z}_m^e$ and $\tilde{Z}_m^h$ are identical to those obtained from the well-known spectral-domain immittance approach [7].

It has been proven in [6] that

$$\sum_{m=1}^{\infty}\overleftrightarrow{H}_m^{\mathrm{T}}(\rho)\ \overleftrightarrow{H}_m\ (\rho') = \frac{\delta(\rho-\rho')}{\sqrt{\rho\rho'}}\ \overleftrightarrow{I} \tag{6}$$

where $\overleftrightarrow{I}$ is the unit dyadic. Based on (6), the following Parseval's relation can be readily derived:

$$\sum_{m=1}^{\infty}\begin{bmatrix} \tilde{E}_m^h & \tilde{E}_m^e \end{bmatrix}\begin{bmatrix} \tilde{J}_m^h \\ \tilde{J}_m^e \end{bmatrix} = \int_0^a \rho\begin{bmatrix} jE_\rho(\rho) & E_\phi(\rho) \end{bmatrix}\begin{bmatrix} jJ_\rho(\rho) \\ J_\phi(\rho) \end{bmatrix}^* d\rho \tag{7}$$

where the superscript * denotes the complex conjugate operation. The results of (7) must vanish because the transversal E-fields and current density functions are zero in complementary regions at $z = h_1 + h_2$ plane. This equation can be used to set up a nonstandard eigenvalue matrix equation, of which the eigenvalue is the resonant frequency of the whole structure, via the use of Galerkin's procedure.

B. Vector Global Basis Functions and Their Hankel Transforms

The unknown currents on the ith ring conductor are expanded as

$$\begin{aligned}\begin{bmatrix} jJ_\rho(\rho) \\ J_\phi(\rho) \end{bmatrix}_i &= \sum_{k=0}^{N_b-1} C_{ik}\begin{bmatrix} \sqrt{1-x_i^2}U_k(x_i) \\ \dfrac{T_k(x_i)}{\sqrt{1-x_i^2}} \end{bmatrix} \\ &\quad + \sum_{k=0}^{N_b-1} d_{ik}\begin{bmatrix} \sqrt{1-x_i^2}U_k(x_i) \\ -\dfrac{T_k(x_i)}{\sqrt{1-x_i^2}} \end{bmatrix}\end{aligned} \tag{8}$$

where $x_i = 2(\rho-\rho_{ci})/w_i$, ρ_{ci} is strip center and w_i the linewidth, T_k and U_k are the Chebyshev polynomials of the first and second kinds, respectively, and c_{ik} and d_{ik} are expansion constants. Note that the important edge conditions for both radial and azimuthal currents have been incorporated into computation.

There are four types of integrals to be evaluated for the Hankel transforms of the vector basis functions in (8). They can be written as

$$\int_{\rho_{ci}-(w_i/2)}^{\rho_{ci}+(w_i/2)}\begin{Bmatrix} J_n(\alpha\rho) \\ \rho J'_n(\alpha\rho) \end{Bmatrix}\begin{Bmatrix} \sqrt{1-x_i^2}U_k(x_i) \\ \dfrac{T_k(x_i)}{\sqrt{1-x_i^2}} \end{Bmatrix} d\rho \tag{9}$$

where α is either λ_m^e or λ_m^h. When the transform kernels J_n and J'_n vary slowly for $|x_i| \le 1$, they are expanded as a series of Chebyshev polynomials of order N_c [9] and the result of (9) can be readily obtained via the orthogonality properties of Chebyshev polynomials with respect to summation. When α is large, the following asymptotic expansions are used [9]:

$$J_n(x) = \sqrt{\frac{2}{\pi x}}\Big[P_n(x)\cos\xi_n(x) - Q_n(x)\sin\xi_n(x)\Big] \tag{10a}$$

$$J'_n(x) = \sqrt{\frac{2}{\pi x}}\Big[R_n(x)\cos\xi_n(x) + S_n(x)\sin\xi_n(x)\Big] \tag{10b}$$

where $\xi_n = x-(2n+1)\pi/4$. $P_n(x)$, $Q_n(x)$, $R_n(x)$, and $S_n(x)$ are expanded by Chebyshev polynomials of argument $8/x$ to represent the magnitudes of the Bessel functions for $x \ge 8$. In this way, the oscillatory part is separated from the integrand and the remaining part

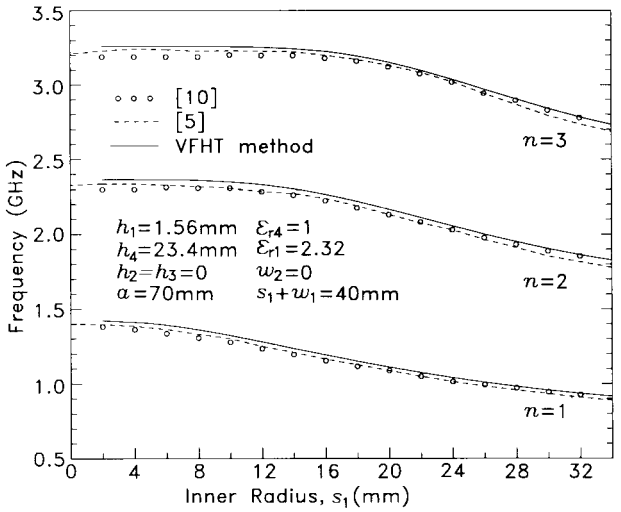

Fig. 2. Validity check of calculated resonant frequencies of microstrip ring resonators.

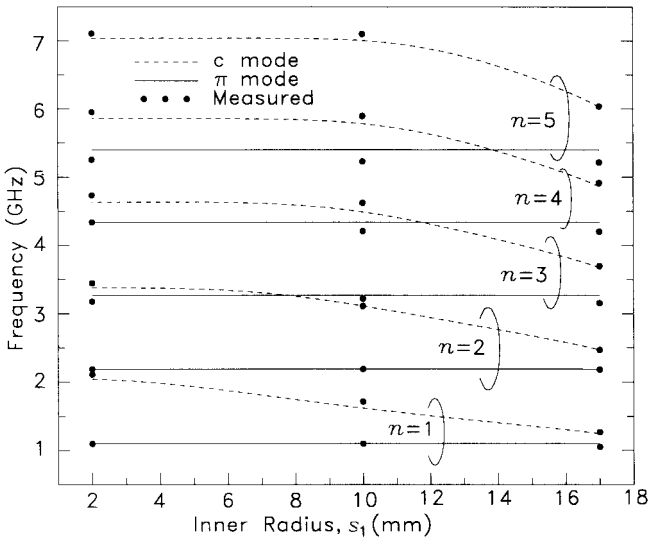

(a)

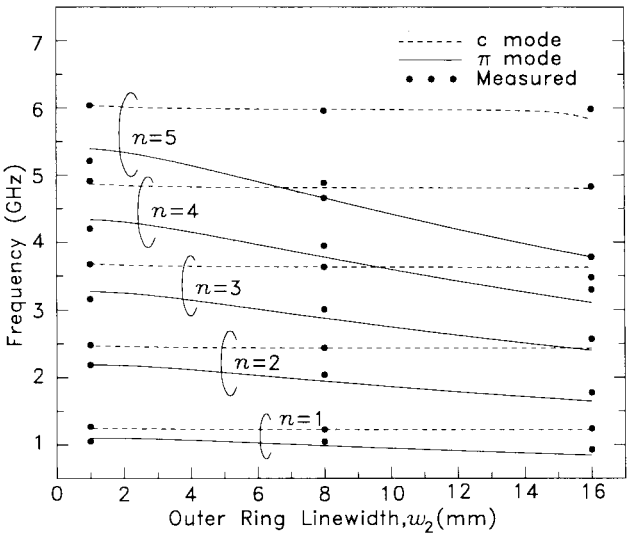

(b)

Fig. 3. Resonant frequencies of coupled microstrip rings in a layered dielectric medium. Structure parameters: $h_1 = 0.508$ mm, $h_2 = 1.27$ mm, $h_3 = 0$, $h_4 = 12.7$ mm, $\varepsilon_{r1} = 2.2$, $\varepsilon_{r2} = 10.2$, $\varepsilon_{r4} = 1$, $a = 50$ mm. (a) $s_1 + w_1 = 18$ mm, $s_2 = 1$ mm, $w_2 = 1$ mm. (b) $s_1 = 17$ mm, $w_1 = 1$ mm, $s_2 = 1$ mm.

can be expanded as a series of Chebyshev polynomials of order N_c. As a result, (9) can be easily obtained by using the following identity:

$$\int_{-1}^{1} \frac{T_m(x)}{\sqrt{1-x^2}} e^{j(\beta x+\theta)} dx = e^{j\theta} \pi (j)^m J_m(\beta) \tag{11}$$

where $\theta = \alpha\rho_{ci} - (2n+1)\pi/4$ and $\beta = \alpha w_i/2$.

III. Results

A. Convergence Behavior of the VFHT and Confidence Check

A single annular ring [5] with $w_1 = 38$ mm, $s_1 = 2$ mm, and $a = 70$ mm is chosen for testing the convergence behavior of the VFHT method. This is a crucial condition for the convergence test because the ring has a wide strip width $w_1 > 0.5a$ and a small inner radius $s_1 < 0.03a$. It is found that $N_c = 48$, $N_b = 7$, and the number of spectral terms $N = 500$ are required to have a 0.1% relative accuracy for this particular case study. We use $N_b = 6$, $N_c = 64$, and $N = 2000$ for all the results presented herein. The size of the final matrix is $2N_b = 12$ for a single-ring resonator. It takes approximately 15 s on an HP735 workstation to calculate one data point.

It is important to check if the converged data obtained by the VFHT is correct. Fig. 2 compares the calculated resonant frequencies with those reported in [5]. The results obtained by the VFHT seem to have 1% deviation from the referred data for all s_1 values. When s_1 is larger than 20 mm, or w_1 is less than 20 mm, the VFHT results have good agreements with the planar waveguide model [10].

B. Some Results and Measurements

Fig. 3(a) and (b) shows the resonant frequencies of a two-ring resonator on a two-layer substrate for the azimuthal resonance order n being from 1 to 5. Two important aspects relevant to this microstrip structure are considered before the investigation of the resonant characteristics is proceeded. First, there are two dominant resonant modes corresponding to the two quasi-TEM modes of straight coupled microstrip transmission lines. Thus, it is possible to use the c and π modes to identify the two dominant resonances. The c mode is referred to that the currents on the coupled rings are of the same polarities and the π mode is to that of opposite polarities. The second aspect is on the stacked dielectric substrates. For straight coupled microstrips on a single-layer substrate, it is known that the even mode has higher effective dielectric constant than the odd mode does. However, on a multilayer substrate, either even or odd mode can have higher $\varepsilon_{\rm reff}$ value than the other one, depending on the substrate height ratio [11]. As a result for the particular structure in Fig. 3, the resonant frequencies for the c mode are higher than those of the π mode.

In Fig. 3(a), the resonant frequencies are plotted against s_1. The linewidth $w_1 = 18 - s_1$ mm. It shows that the π-mode results are nearly independent of the variation of s_1, while the c-mode frequencies increase when s_1 is decreased. When $s_1 = 17$ mm and $w_1 = 1$ mm, the resonant frequencies for both modes with $n \geq 2$ are close to n times the values with $n = 1$. This situation does not apply to that with $s_1 = 2$ mm and $w_1 = 16$ mm due to the curvature effect. In Fig. 3(b), the resonant frequencies are calculated for w_2, varying from 1 to 16 mm with $w_1 = s_2 = 1$ mm. The π-mode results decrease as w_2 is increased, while the c-mode frequencies are insensitive to the variation of w_2.

The measured circuits were fabricated on RT/Duroid 6010.2 ($\varepsilon_r = 10.2$) and 5880 ($\varepsilon_r = 2.2$) substrates. For the tradeoff between the insertion loss and perturbation of the experimental structure: 1) the loose coupling scheme [1] with a coupling gap of 0.254 mm (10 mil) is used and 2) collinear 50-Ω feeding and extracting microstrip lines are designed in the circuits. In measurements, the modes are identified by comparing the results with the simulated data. The measured resonant frequencies for the coupled microstrip rings show good agreement with the prediction by the VFHT.

IV. Conclusion

The VFHT is formulated for characterizing shielded single and coupled microstrip ring resonators in an inhomogeneous medium. With variational nature, the method can provide nearly converged results by using several hundreds of summation terms. The calculation resonant frequencies and the measurements have good agreements. The technique can be extended to deal with annular slot, disk, and multiple annular-ring resonators embedded in a multilayer structure.

References

[1] K. Chang, *Microwave Ring Circuits and Antennas.* New York: Wiley, 1996.

[2] S. G. Pintzos and R. Pregla, "A simple method for computing the resonant frequencies of microstrip ring resonators," *IEEE Trans. Microwave Theory Tech.*, vol. MTT-26, pp. 809–813, Oct. 1978.

[3] K. Araki and T. Itoh, "Hankel transform domain analysis of open circular microstrip radiating structures," *IEEE Trans. Antennas Propagat.*, vol. AP-29, pp. 84–89, Jan. 1981.

[4] S. M. Ali, W. C. Chew, and J. A. Kong, "Vector Hankel transform analysis of annular-ring microstrip antenna," *IEEE Trans. Antennas Propagat.*, vol. AP-30, pp. 637–644, July 1982.

[5] F. Tefiku and E. Yamashita, "An efficient method for the determination of resonant frequencies of shielded circular disk and ring resonators," *IEEE Trans. Microwave Theory Tech.*, vol. 41, pp. 343–346, Feb. 1993.

[6] W. C. Chew and T. M. Habashy, "The use of vector transforms in solving some electromagnetic scattering problems," *IEEE Trans. Antennas Propagat.*, vol. AP-34, pp. 871–879, July 1986.

[7] T. Itoh, "Spectral domain immittance approach for dispersion characteristics of generalized printed transmission lines," *IEEE Trans. Microwave Theory Tech.*, vol. MTT-22, pp. 733–736, July 1980.

[8] C.-T. Tai, *Dyadic Green Functions in Electromagnetic Theory*, 2nd ed. Piscataway, NJ: IEEE Press, 1994, ch. 6.

[9] C. W. Clenshaw, *National Physical Laboratory Mathematical Tables, vol. 5* (Chebyshev Series for Mathematical Functions). London, U.K.: Her Majesty's Stationery Office, 1962.

[10] A. M. Khilla, "Computer-aided design for microstrip ring resonators," in *Proc. 11th European Microwave Conf.*, Amsterdam, The Netherlands, 1981, pp. 1–6.

[11] J. P. K. Gilb and C. A. Balanis, "Asymmetric, multiconductor low-coupling structures for high-speed high-density digital interconnects," *IEEE Trans. Microwave Theory Tech.*, vol. 39, pp. 2100–2106, Dec. 1991.

Mutual Coupling Between Millimeter-Wave Dielectric-Resonator Antennas

Yong-Xin Guo, Kwai-Man Luk, and Kwok-Wa Leung

***Abstract*— The mutual coupling between aperture-coupled cylindrical dielectric-resonator antennas (DRA's) is analyzed using the finite-difference time-domain method. The perfectly matched layer is used as absorbing boundary conditions. The voltage excitation source of microstrip structure is based on the Zhao's model, in which the source plane or the terminal plane can be moved very close to the discontinuity so that the computational domain can be reduced substantially. The numerical results are verified by measurements and reasonable agreement between theory and experiment is obtained. It is shown that this method is highly efficient for the analysis of DRA's.**

***Index Terms*—Dielectric antennas, FDTD methods, mutual coupling.**

I. Introduction

Dielectric-resonator antennas (DRA's) have been considered for applications at millimeter-wave frequencies since systematic experimental investigations on DRA's were carried out by Long *et al.* [1]. DRA's share many of the advantages of microstrip antennas, including small size, low profile, light weight, ease of coupling to almost all types of transmission lines, and ease of integration with other active or passive microwave integrated circuit (MIC) components. In addition, DRA's avoid the inherent disadvantages of patch antennas, such as high conduction loss at millimeter-wave frequencies, narrow bandwidth, and low efficiency due to surface-wave excitation. Most of the available theoretical and experimental investigations on DRA's are on an isolated element of various shapes [1]–[3]. Among the various excitation methods for DRA's, the aperture-coupled feed is most welcome since it can be practically implemented at high frequencies and is suitable for monolithic-microwave integrated-circuit (MMIC) applications [2], [3]. In some applications, a number of DRA's are combined to form an array for high gain requirement. Several designs of probe-fed DRA arrays are reported in the literature [4], [5]. However, very few investigations have been undertaken to assess the performance of an aperture-coupled DRA array, and only a few experimental results have been reported [6]–[8].

In this paper, the mutual coupling of aperture-coupled cylindrical dielectric-resonator arrays (CDRA's) using the finite-difference time-domain (FDTD) method with Berenger's perfectly matched layer (PML) absorbing boundary condition (ABC) is studied because it is a crucial parameter in evaluating the performance of an antenna array. The advantage of this approach is the ability to investigate basic structures, as well as more complicated DRA's, which are hardly analyzed by the previous methods [2], [3]. The DRA's are operated at the fundamental broadside $\mathrm{TM}_{11\delta}$ mode [1]. Besides, the reflection coefficients of the CDRA's are presented for completeness. Measurements have been conducted to validate the calculations.

II. Theory

The three-dimensional (3-D) FDTD algorithm is applied to analyze the CDRA's. A detailed description of the FDTD method will be

Manuscript received January 19, 1999. This work was supported by the Research Grant Council, Hong Kong, under Project 9040165.

The authors are with the Department of Electronic Engineering, City University of Hong Kong, Kowloon, Hong Kong, China.

Publisher Item Identifier S 0018-9480(99)08795-5.